Direct calculation of interfacial energetics: Roles of axial commensuration and strain in epitaxial growth

Akiko Kobayashi and S. Das Sarma
Department of Physics and Astronomy, University of Maryland, College Park, Maryland 20742
(Received 20 October 1986)

Static energetics of monolayer overgrowth on a crystalline substrate is considered in detail by going beyond the rigid-lattice approximation. Conditions necessary to obtain a coherent interface between two dissimilar structures are carefully examined in terms of axial commensuration. Obtaining the strain and the strain energy for lattice-mismatched interfaces, we investigate: (i) the nucleation size for stable microcrystallite formation, and (ii) the difference in epitaxial growth between positive misfit and negative misfit. Using model potentials obtained by superposing suitable two-body interaction terms, we make a connection with semiconductor superlattice growth for zinc-blende-type systems.

I. INTRODUCTION

Starting with the pioneering work of Frank and van der Merwe,[1] energetics studies of the epitaxial growth of a thin film on a crystalline substrate have provided an important basis for dealing with interface stability, strain effects, dislocation formation, growth modes, and various other structural properties pertaining to surfaces, interfaces, and superlattices. Both theoretical and experimental efforts have been made to study these properties in a variety of systems. Some examples are deposition of a noble gas (Ar, Xe, Kr, . . .) on graphite[2–6] and on metals (W, Cu, Ag, . . .),[7,8] Ag on a Si surface,[9] Al on a Ge surface,[10] Al and Sb on a GaAs surface,[11–15] metal on metal (Ta/Nb, Cu/Nb, Mo/V, Ni/Mo, . . .),[16–20] and semiconductor on semiconductor (AlAs/GaAs, InAs/GaSb, Ge/GaAs, $GaP/GaAs_{1-x}P_x$, $Ga_{1-x}In_xAs/GaAs$, . . .).[21–23] Obtaining a complete understanding of interface formation, however, is a formidable undertaking because of the lack of precise knowledge of the nature of the microscopic interaction among constituent atoms and because of the complex kinetic processes that occur during growth (such as diffusion, chemical reaction, and evaporation of adatoms). In modern crystal growth techniques (such as molecular-beam epitaxy or metalorganic chemical-vapor deposition), many of the growth parameters are controllable, but their precise roles in affecting the diverse phenomena at growth fronts are unknown. In view of these complexities, epitaxial growth theory within the framework of the classical treatment[1,24,25] can be regarded as a guideline towards a qualitative understanding of structural properties of surfaces, interfaces, and superlattices (and towards an eventual efficient exploitation of these growth techniques).

Nucleation of microcrystallites, which is usually followed by coalescence and reorientation of these entities, seems to be an important phase in determining the epitaxy.[25,26] In order to obtain some insight into interface formation, we focus on the structural meaning of the epitaxy and the effects of size on nucleation, by considering the static energetics of monolayer overgrowth on a crystalline substrate. We use a simple and direct method: basically an appropriate summation of interatomic potentials over an underlying structure, including only two-body interactions. Obvious shortcomings of this method are (i) it is not feasible to list energy values quantitatively, and (ii) the two-body interatomic potential is not suitable for dealing with semiconductor systems, since it excludes the formation of tetrahedral bonding from the melt.[27,28] However, by explicitly neglecting the contributions arising from more than two-body interactions, an investigation of the dependence of interface energetics on a variety of important variables is tractable. The present approach is, therefore, complementary to, for example, first-principles total energy calculations.

The rest of this paper consists of two parts. In Sec. II the possibility of obtaining a coherent interface between two dissimilar structures (that differ in symmetry) is investigated, assuming that both the adsorbate and substrate are rigid (rigid-lattice approximation[1,19,24]). By examining the dependence of total energy on adsorbate-cluster size, we obtain the conditions for coherency in terms of axial commensuration between the two structures. As specific examples, the systems fcc(111)/bcc(110), fcc(111)/fcc(001), and fcc(111)/fcc(110) are considered. Section III is devoted to the study of strain at lattice-mismatched interfaces and its subsequent role in nucleation and growth. The nucleation size of a stable cluster is obtained by determining the critical size for the onset of pseudomorphism. The difference in epitaxial growth between positive misfit and negative misfit is discussed by explicitly taking into account an anharmonic force in the adsorbate monolayer. We go beyond the rigid-lattice approximation in these calculations and consider explicitly both the adsorbate-adsorbate and adsorbate-substrate interactions.

II. CONDITIONS FOR INTERFACE COHERENCY OF TWO DISSIMILAR STRUCTURES

A. Outline of calculation

We obtain the total energies of interfaces composed of two structures that differ in symmetry, as a function of the basic variables: the lattice-constant ratio, relative orientation, and relative displacement between the adsorbate and the substrate. We employ the rigid-lattice approximation,[1,19,24] in which both the adsorbate and substrate are assumed to be rigid so that the only interaction to be considered is that operating between adsorbate and substrate atoms. By reading off the values of the above basic variables that pertain to the total energy minimum, the present calculation should serve as a convenient touchstone for a preliminary check on the possibility of obtaining a coherent interface between two dissimilar materials. We consider specifically the systems fcc(111)/bcc(110), fcc(111)/fcc(001), and fcc(111)/fcc(110): the two-dimensional unit cell of each of these structures is shown in Fig. 1.

Provided that an appropriate functional form for the interatomic potential is available, the total energy per adsorbate atom within the rigid-lattice approximation is simply expressed as

$$E=\frac{1}{N}\sum_{a}\sum_{s}u(|\mathbf{r}_a-\mathbf{r}_s|)\,, \tag{1}$$

where $u(|\mathbf{r}_a-\mathbf{r}_s|)$ is the interatomic potential between an adsorbate atom at the site $\mathbf{r}_a$ and a substrate atom at the site $\mathbf{r}_s$, and N is the total number of adsorbate atoms. Note that, because of the translational invariance of the substrate surface, the substrate potential seen by a single adatom, i.e., $V(\mathbf{r})=\sum_s u(|\mathbf{r}-\mathbf{r}_s|)$, has the following property:

$$V(\mathbf{r}+\mathbf{R}_s)=V(\mathbf{r})\,, \tag{2}$$

where $\mathbf{R}_s$ is the two-dimensional lattice vector of the substrate. $V(\mathbf{r})$ can therefore be cast into a Fourier representation using the two-dimensional reciprocal lattice vector, $\mathbf{G}_s$, of the substrate. As a result, the total energy can be written in the form

$$E=\frac{1}{N}\sum_{s}V_F(\mathbf{G}_s)\Big[\sum_{a}\exp(i\mathbf{G}_s\cdot\mathbf{r}_a)\Big]\,, \tag{3}$$

where $V_F(\mathbf{G}_s)$ is the Fourier coefficient of the substrate potential $V(\mathbf{r})$.

We use the following form of a two-body interatomic potential for $u(|\mathbf{r}_a-\mathbf{r}_s|)$:

$$u(r)=4\epsilon\exp\left\{-\frac{8}{3}\left[\left(\frac{r}{\sigma}\right)^2-1\right]\right\}\times\left[\exp\left\{-\frac{8}{3}\left[\left(\frac{r}{\sigma}\right)^2-1\right]\right\}-1\right]. \tag{4}$$

In the above short-range exponentially decaying potential,[19] the parameters ϵ and σ play a role similar to the corresponding parameters in the Lennard-Jones (6-12) potential. Namely, the potential has a minimum value, ϵ, at a distance $\cong 1.12\sigma$, and there exists a high hard-core barrier for $r<\sigma$. However, the potential in Eq. (4) approaches zero with increasing r faster than the Lennard-Jones potential. Using Eq. (4) for $u(|\mathbf{r}-\mathbf{r}_s|)$, the Fourier transform of $V(\mathbf{r})$, i.e., $V_F(\mathbf{G}_s)$ in Eq. (3), has a simple exponential form.

In employing the interatomic potential in the form of Eq. (4), we note that the quantity 1.12σ can be naturally

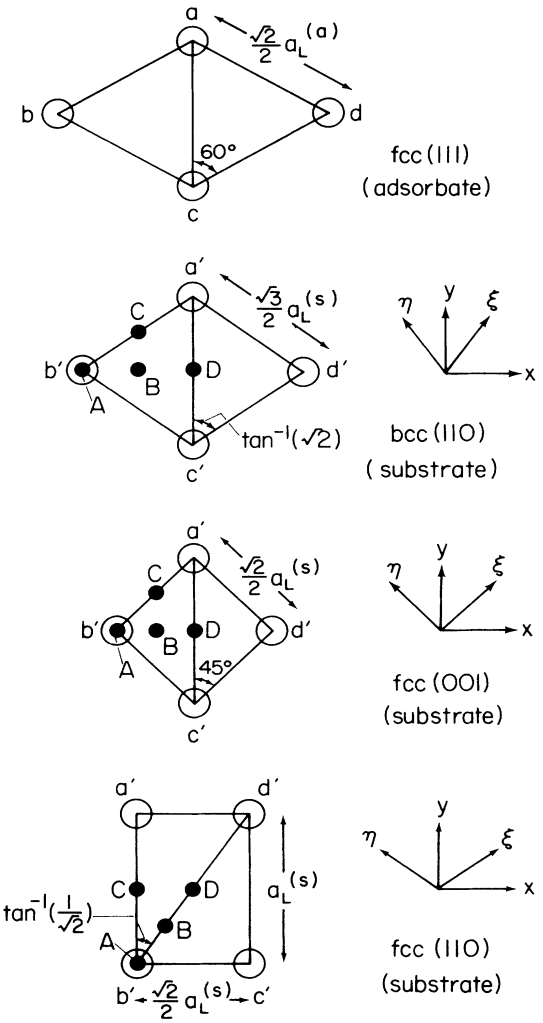

FIG. 1. Two-dimensional unit cell of each of the structures fcc(111), bcc(110), fcc(001), and fcc(110). Open circles, denoted by a, b, c, and d for fcc(111), and those by a', b', c', and d' for the other three structures represent the positions of atoms in a unit cell. Solid circles, denoted by A, B, C, and D, refer to the positions of the central atom of the adsorbate cluster with respect to each of the substrate unit cells (relative displacement). The edge length of each unit cell is shown in terms of the lattice constant $a_L^{(a)}$ for the adsorbate and $a_L^{(s)}$ for the substrate. The axes drawn on the right-hand side of each substrate specify the relevant directions for axial commensurations (see the text). The ξ axis is perpendicular to $b'c'$, and the η axis is perpendicular to $a'b'$ for bcc(110) and fcc(001). For fcc(110), the ξ axis is perpendicular to $a'c'$, and the η axis is perpendicular to $b'd'$.

interpreted as the approximate first-nearest-neighbor bondlength of the bulk, if the adatoms are a constituent of the substrate (e.g., Ni on Ni substrate) and if we ignore surface reconstruction. Assigning specific values to the parameters is thus equivalent to defining an appropriate position for an adatom to be in registry with the substrate. To make the fitting flexible, we extend the interatomic potential in Eq. (4) to the anisotropic case:

$$\left[\frac{r}{\sigma}\right]^2 \rightarrow \left[\frac{x}{\sigma_x}\right]^2 + \left[\frac{y}{\sigma_y}\right]^2 + \left[\frac{z}{\sigma_z}\right]^2 . \tag{5}$$

It is found that, for a bcc(110) substrate, it takes up to the second Fourier term to confirm energy convergence and the relationships: $1.12\sigma_x \cong a_L^{(s)}$, $1.12\sigma_y \cong (\sqrt{2}/2)a_L^{(s)}$, and $1.12\sigma_z \cong a_L^{(s)}$, where $a_L^{(s)}$ is the lattice constant of the substrate. For fcc(001), it takes up to the second Fourier term to confirm energy convergence and the relationships: $1.12\sigma_x = 1.12\sigma_y = 1.12\sigma_z \cong (\sqrt{2}/2)a_L^{(s)}$. For fcc(110), it takes up to the third Fourier term to confirm energy convergence and the relationships: $1.12\sigma_x = 1.12\sigma_y = 1.12\sigma_z \cong (\sqrt{2}/2)a_L^{(s)}$. Inclusion of more than the first layer of the substrate is not necessary, since the effects of all other substrate layers in determining the specific position for an adatom are simulated in the parameters σ_x, σ_y, and σ_z as in the above.

The crystallographic relationships between the adsorbate [fcc(111)] and the substrate [bcc(110), fcc(001), or fcc(110)] can be seen in Fig. 1 The open circles, denoted by a, b, c, and d for the adsorbate, and by a', b', c', and d' for the substrate, represent the positions of atoms in the two-dimensional unit cell of each of the structures. The unit cell of the fcc(111) structure shown in Fig. 1 refers to the case of zero relative orientation with respect to the substrate [$ac||a'c'$ for fcc(111)/bcc(110) and fcc(111)/fcc(001); $ac||a'b'$ for fcc(111)/fcc(110)]. We define a finite relative orientation, θ, as a counter-clockwise rotation of the adsorbate with respect to the configuration drawn in Fig. 1. In defining the rotation, the position of the "origin" of the adsorbate needs to be defined simultaneously. The solid circles, denoted by A, B, C, and D, on the unit cell of each substrate refer to the representative positions of the central atom of the adsorbate with respect to the substrate (relative displacement). The edge length of each unit cell is shown in Fig. 1 in terms of the lattice constant $a_L^{(a)}$ for the adsorbate and $a_L^{(s)}$ for the substrate. Total energies of the systems are calculated as a function of lattice-constant ratio $a_L^{(a)}/a_L^{(s)}$ and relative orientation θ for the cases of relative displacement specified as A, B, C, and D above. We vary the total number of adsorbate atoms between $\cong 10$ and $\cong 10^4$ to study the size dependence of the total energy. Because of our use of Fourier representation, the substrate is effectively infinite in size.

B. Results and discussion

1. fcc(111)/bcc(110)

In Fig. 2 we display the resulting energies per adsorbate atom versus $a_L^{(a)}/a_L^{(s)}$ for the interface composed of an fcc(111)—adsorbate monolayer and a bcc(110)—substrate, with fixed relative orientation $\theta = 0°$. The energies corresponding to four different relative displacements A, B, C, and D are indicated by solid, dashed, broken, and dotted lines, respectively. The energies were calculated for three different values of the total number of adsorbate atoms, $N = 121$, 441, and 2601. In all cases, the energies were found to converge at $z \cong 0.9a_L^{(s)}$ above the substrate sur-

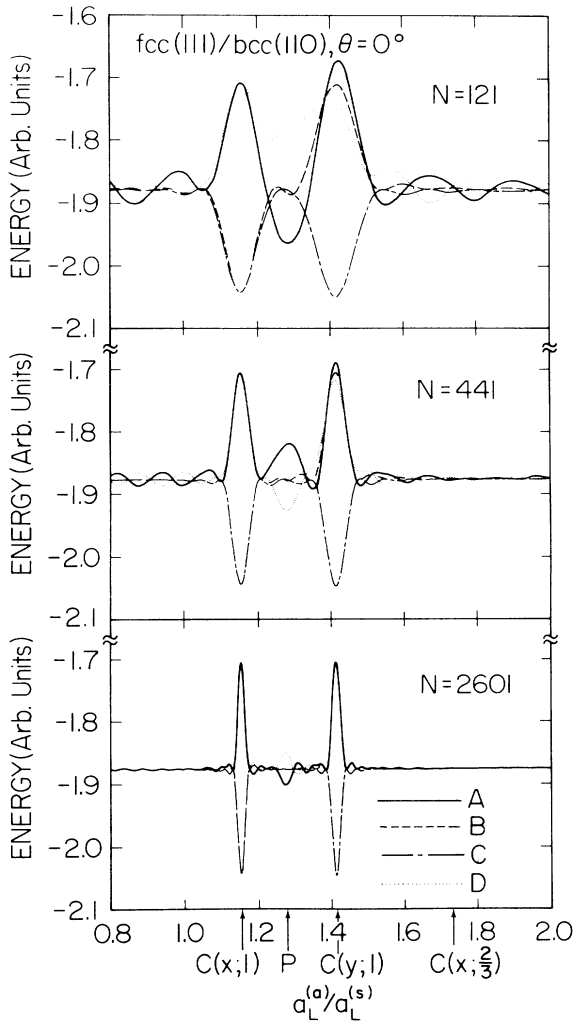

FIG. 2. Energies per adsorbate atom of the system fcc(111)/bcc(110), as a function of lattice-constant ratio $a_L^{(a)}/a_L^{(s)}$, with fixed relative orientation $\theta = 0°$. The energies corresponding to four different relative displacements (i.e., the central atom of the adsorbate with respect to the substrate being at position A, B, C, or D as specified in Fig. 1) are indicated by solid, dashed, dashed-dotted, and dotted lines, respectively. The energies are calculated for three different values of the total number of adsorbate atoms, $N = 121$, 441, and 2601. $C(x;n/m)$ and $C(y;n/m)$ (n, m are integers) indicate the direction and the order of axial commensuration. P indicates partial commensuration. See the text for the detailed discussion.

face. Features that can be noticed in Fig. 2 are (i) there are two main peaks at $a_L^{(a)}/a_L^{(s)} \cong 1.15$ and 1.41, whose linewidths become smaller with increasing N; (ii) secondary peaks, distinct in the spectra for small-cluster size, seem to diminish with increasing N, except the small peak at $a_L^{(a)}/a_L^{(s)} \cong 1.27$; and (iii) the energy depends sensitively on the "origin" of the adsorbate cluster—for example, a cluster with $a_L^{(a)}/a_L^{(s)} \cong 1.15$ and $\theta = 0°$ is stable when the central adsorbate atom is at position B or C, whereas the same cluster but with different relative displacement (A or D) gives rise to an energy maximum instead of minimum.

Although not shown here, we found that the energy spectra for $N \cong 10^4$ exhibit strong δ-function-like peaks at $a_L^{(a)}/a_L^{(s)} \cong 1.15$ and 1.41, and a very weak (but nonvanishing) δ-function-like peak at $\cong 1.27$, with no secondary peaks. The widths of the two main peaks are found to vary as $\propto N^{-1/2}$. Based on these trends of the energy spectra as N is increased, we conclude that the finite widths of the two main peaks and the appearance of the secondary peaks are caused by edge effects due to the finite-size adsorbate cluster. Note that these are observable finite-size effects in an actual experimental system, not an artifact arising from the finite-cluster calculation.

The dependence of energy on relative displacement has been reported previously,[29] employing the Lennard-Jones potential for an interface composed of an adsorbate with 127 atoms and a substrate comprised of 441 atoms per monolayer with a total of four monolayers stacked normal to the growth axis. The present calculation, which enables us to deal with any size of adsorbate cluster, clearly shows that the origin dependence does not arise from the finite-size effect. Indeed, the peak positions, $a_L^{(a)}/a_L^{(s)} = 2/\sqrt{3}$ ($\cong 1.15$) and $\sqrt{2}$ ($\cong 1.41$), together with the strong dependence of energy values on relative displacement at these points, signify the importance of crystallographic relationships between the adsorbate and substrate in determining stability conditions (and eventual successful growth of coherent interfaces); that is, axial commensuration. Using the geometry of Fig. 1 (case of $\theta = 0°$), we see that, if the lattice-constant ratio is such that atomic positions on the fcc(111) mesh are incommensurate with those on the bcc(110) mesh, the substrate-potential strength experienced by each adsorbate atom differs from position to position so as to fill in the entire potential well within a substrate unit cell (in the limit of infinite number of adsorbate atoms). The energy per adsorbate atom is thus effectively the average value of the potential-well depth (incommensuration energy). In Fig. 2 the energy value to which the secondary peaks converge ($\cong -1.85$ in units where $\epsilon = 1$) corresponds to such an average value of the potential-well depth in a bcc(110) unit cell. On the other hand, axial commensuration can be realized when the ratio between the length of ac (bd) and that of $a'c'$ ($b'd'$) becomes a rational number. In the case of $ac = a'c'$, i.e., $a_L^{(a)}/a_L^{(s)} = \sqrt{2}$, the atomic positions of the adsorbate on the row along bd and those of the substrate on the row along $b'd'$ are incommensurate with each other, but these incommensuration lines along the x direction form a laterally periodic and commensurate array perpendicular to the row direction (y direction). In Fig. 2, $C(y;1)$ denotes the above situation, namely axial commensuration along the y direction with the condition that the spacing of the parallel rows of adsorbate atoms (along the x direction) is equal to the spacing of the parallel rows of the substrate atoms (along the x direction). The relative displacement thus plays an important role in determining the energy pertaining to axial commensuration. In the case of $C(y;1)$, since the atomic positions along the x direction are incommensurate, the displacement of the adsorbate along the x direction does not change the energy, giving rise to the same value for the cases of the central adsorbate atom being at position A, B, or D. The energy is the lowest when the central adsorbate atom is at position C, because each of the rows of adsorbate atoms passes through a trough located halfway between the rows of substrate atoms, where the potential is most attractive.

Likewise, $C(x;1)$ denotes the situation in which the incommensuration lines of the adsorbate and the substrate along the y direction form a commensurate array along the x direction with the condition $bd = b'd'$ (i.e., $a_L^{(a)}/a_L^{(s)} = 2/\sqrt{3}$). The adsorbate cluster with the relative displacement A (B) and that with D (C) are thus equivalent. The energy is the lowest when the parallel rows of adsorbate atoms are located alternately with the rows of substrate atoms (i.e., the case of relative displacement B or C).

In the region $0.8 \leq a_L^{(a)}/a_L^{(s)} \leq 2.0$, there exists another type of axial commensuration, which is denoted by $C(x;\frac{2}{3})$ in Fig. 2. This is the axial commensuration along the x direction with the condition $2bd = 3b'd'$ (i.e., $a_L^{(a)}/a_L^{(s)} = \sqrt{3}$). The energy value pertaining to it, however, is indistinguishable from the incommensuration energy. This is due to the form of the potential chosen in the present calculation. In an actual material, the energy for $C(x;\frac{2}{3})$ may be different from the incommensuration energy, but the difference would be very small as compared to the case of $C(x;1)$ or of $C(y;1)$.

The small peak at $a_L^{(a)}/a_L^{(s)} \cong 1.27$ is interesting. As mentioned earlier, this peak has a very weak but nonvanishing intensity for $N \cong 10^4$, with relative displacement D giving the minimum. The geometrical relationship between the fcc(111) and bcc(110) for this case can be seen with the aid of the axes drawn on the right-hand side of the bcc(110) structure in Fig. 1: the $\xi(\eta)$ axis is perpendicular to $b'c'$ ($a'b'$). This peak corresponds to a situation in which the projection of ab (bc) and that of $a'b'$ ($b'c'$) on to the $\xi(\eta)$ axis become equal, giving the relationship, $a_L^{(a)}/a_L^{(s)} = 4/(\sqrt{3}+\sqrt{2}) \cong 1.27$. Incommensuration occurs in both x and y directions. Therefore, this type of relationship may be called "partial commensuration," and is denoted by "P" in Fig. 2. Although the energy gain arising from the configuration P is definitely smaller than that of $C(x;1)$ or $C(y;1)$, it appears possible to have a semistable interface composed of fcc(111) and bcc(110) with the relationship $a_L^{(a)}/a_L^{(s)} \cong 1.27$ and $\theta = 0°$. However, as can be seen from the origin dependence of energy for different N's in Fig. 2, the adsorbate cluster, as it grows, undergoes translational motion as $ADAD\cdots$ so as to attain the energetically favorable position. Since the position of the central atom (either A or D) can be in a nearest-neighbor cell with respect to the previous cell, the

cluster would exhibit a highly mobile aspect as it grows: this could pose difficulty in coalescing with nearby clusters.

On the basis of the geometrical considerations and the static energies calculated in the present method, we can conclude that obtaining a coherent interface between two dissimilar structures is possible only when the adsorbate and substrate materials are selected so that axial commensuration can be attained. It should be mentioned here that the dependence of energy on relative displacement as well as on cluster size have been left out of the rather extensive literature on epitaxial energetics.[19,24] We note that the role played by axial commensuration becomes transparent only when these factors are taken into consideration.

It can be seen immediately that, in addition to the case of relative orientation $\theta=0°$, axial commensuration can occur when $\theta=60°-\tan^{-1}(\sqrt{2})\cong 5.3°$ and $\theta=30°$. When $\theta\cong 5.3°$, ab becomes parallel to $a'b'$. Thus one can expect the occurrence of first-order η-axial commensuration,

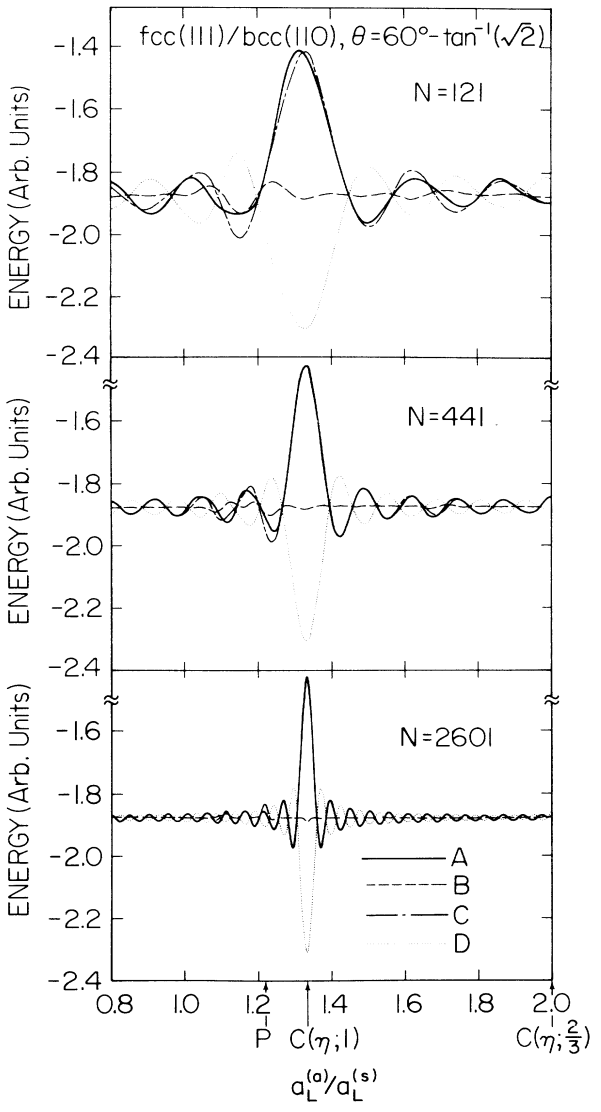

FIG. 3. Energies per adsorbate atom of the system fcc(111)/bcc(110) as a function of lattice-constant ratio $a_L^{(a)}/a_L^{(s)}$, with fixed relative orientation $\theta=60°-\tan^{-1}(\sqrt{2})$, for the total number of adsorbate atoms, $N=121$, 441, and 2601. The energies corresponding to four relative displacements, A, B, C, and D (see Fig. 1), are indicated by solid, dashed, dashed-dotted, and dotted lines, respectively. $C(\eta;n/m)$ (n, m are integers) indicates η-axial commensuration and its order. P indicates partial commensuration. See the text for the detailed discussion.

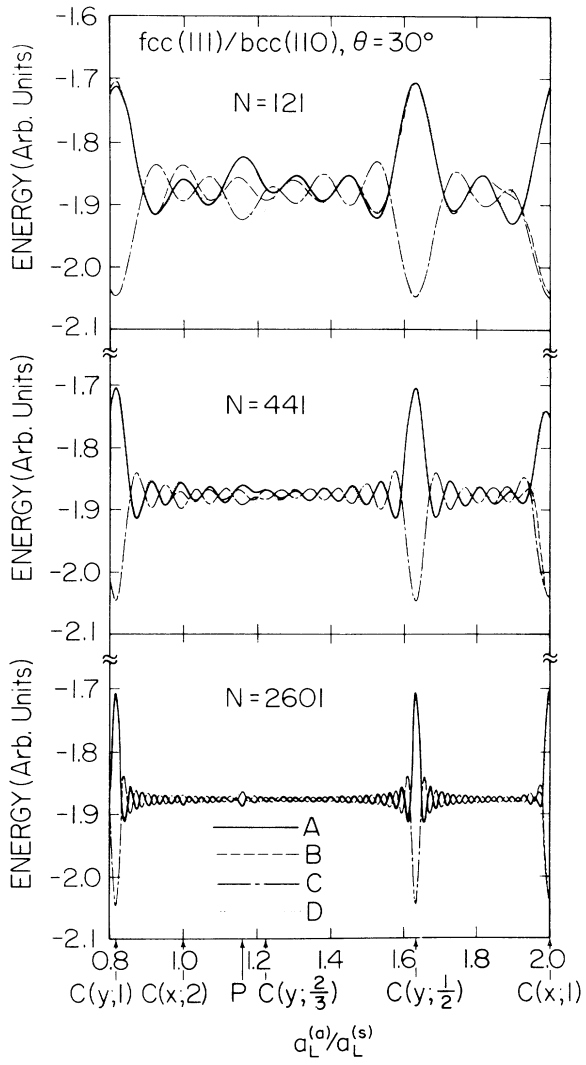

FIG. 4. Energies per adsorbate atom of the system fcc(111)/bcc(110), as a function of lattice-constant ratio $a_L^{(a)}/a_L^{(s)}$, with fixed relative orientation $\theta=30°$, for the total number of adsorbate atoms, $N=121$, 441, and 2601. The energies corresponding to four different relative displacements, A, B, C, and D (see Fig. 1), are indicated by solid, dashed, dashed-dotted, and dotted lines, respectively. $C(x;n/m)$ and $C(y;n/m)$ (n, m are integers) indicate the direction and the order of axial commensuration. P indicates partial commensuration. See the text for the detailed discussion.

$C(\eta;1)$, when the spacing between the ab row and cd row becomes equal to the spacing between the $a'b'$ row and $c'd'$ row, i.e., $a_L^{(a)}/a_L^{(s)}=\frac{4}{3}$. This relationship gives rise to a distinct peak in energy as depicted in Fig. 3. The energy minimum can be attained only when the central atom is at position D, since each of the rows of adsorbate atoms passes through a trough located halfway between the rows of substrate atoms. The secondary peaks due to the finite-size effect seen in Fig. 3 seem to persist even for fairly large cluster size as compared to the case of $\theta=0°$ (Fig. 2). We also notice that the peak intensity for $C(\eta;1)$ is stronger than that for $C(x;1)$ or $C(y;1)$ in Fig. 2. These features arise from the fact that the difference between the substrate potential maximum and minimum seen by each of the adsorbate rows is larger for $\theta\cong 5.3°$ than $\theta=0°$. This can be seen, for example, from the case of $C(\eta;1)$ with relative displacement D, where each adsorbate row along ab (or cd) passes through the absolute

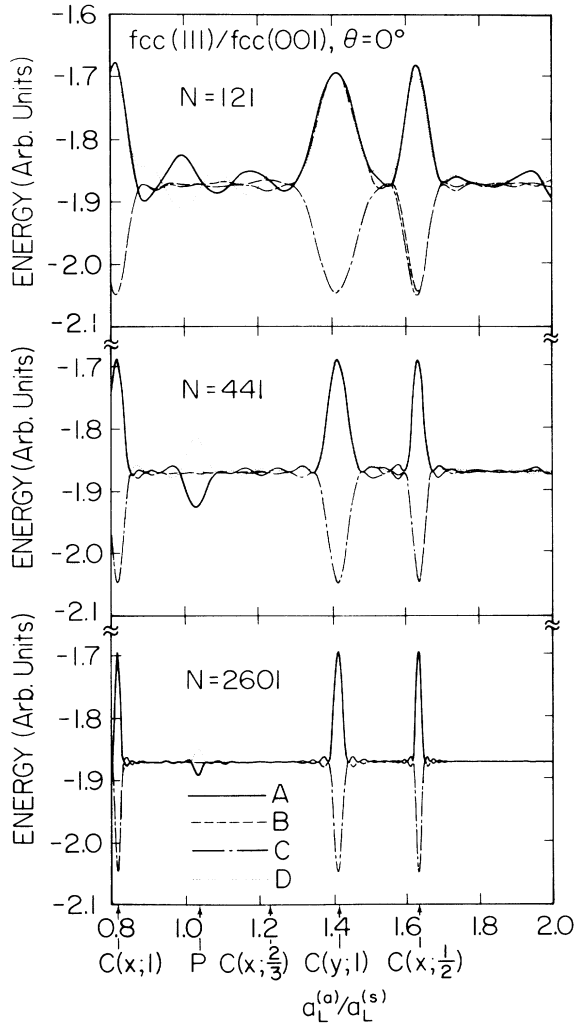

FIG. 5. Energies per adsorbate atom of the system fcc(111)/fcc(001) as a function of lattice-constant ratio, $a_L^{(a)}/a_L^{(s)}$, with fixed relative orientation $\theta=0°$, for the total number of adsorbate atoms, $N=121$, 441, and 2601. The energies corresponding to four relative displacements, A, B C, and D (see Fig. 1), are indicated by solid, dashed, dashed-dotted, and dotted lines, respectively. $C(x;1)$, at $a_L^{(a)}/a_L^{(s)}=2/\sqrt{6}\cong 0.82$, $C(y;1)$ at $\sqrt{2}\cong 1.41$, $C(x;\frac{2}{3})$ at $3/\sqrt{6}\cong 1.22$, and $C(x;\frac{1}{2})$ at $4/\sqrt{6}\cong 1.63$ indicate the direction and the order of axial commensuration. P at $a_L^{(a)}/a_L^{(s)}=4/(\sqrt{6}+\sqrt{2})\cong 1.035$ indicates partial commensuration, in which the projection of ab onto the ξ axis becomes equal to that of $a'b'$ (simultaneously, the projection of ad onto the η axis becomes equal to that of $a'd'$).

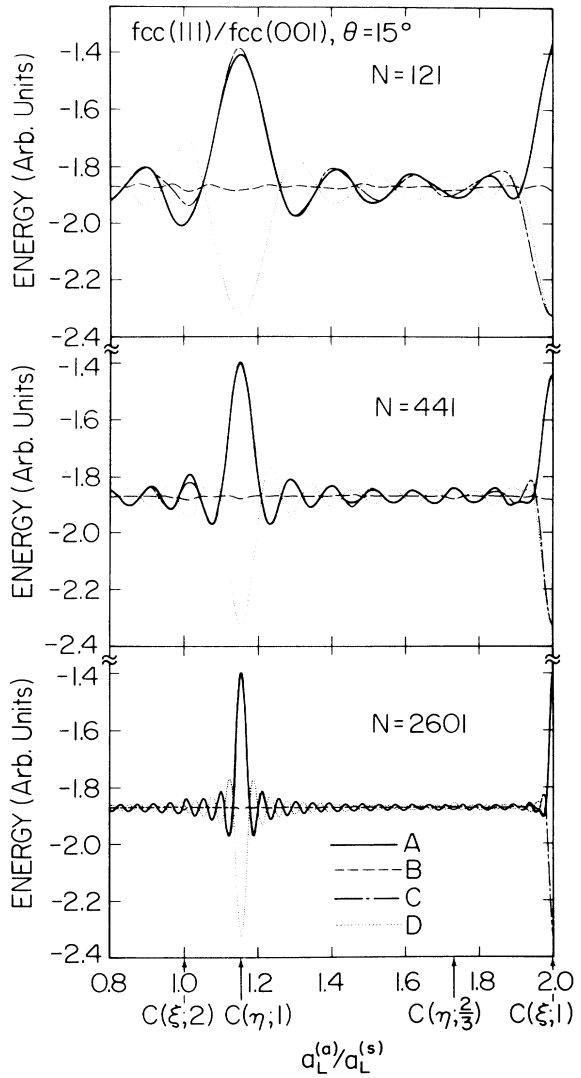

FIG. 6. Energies per adsorbate atom of the system fcc(111)/fcc(001), as a function of lattice-constant ratio $a_L^{(a)}/a_L^{(s)}$, with fixed relative orientation $\theta=15°$, for the total number of adsorbate atoms, $N=121$, 441, and 2601. The energies corresponding to four relative displacements, A, B, C, and D (see Fig. 1) are indicated by solid, dashed, dashed-dotted, and dotted lines, respectively. $C(\xi;2)$ at $a_L^{(a)}/a_L^{(s)}=1$, $C(\xi;1)$ at 2, $C(\eta;1)$ at $2/\sqrt{3}\cong 1.15$, and $C(\eta;2/3)$ at $\sqrt{3}\cong 1.73$ indicate the direction and the order of axial commensuration.

potential minimum of each substrate unit cell, whereas, in the cases of $C(x;1)$ with relative displacement B or C, each adsorbate row passes through a point located a quarter distance away from the absolute potential minimum in a substrate unit cell.

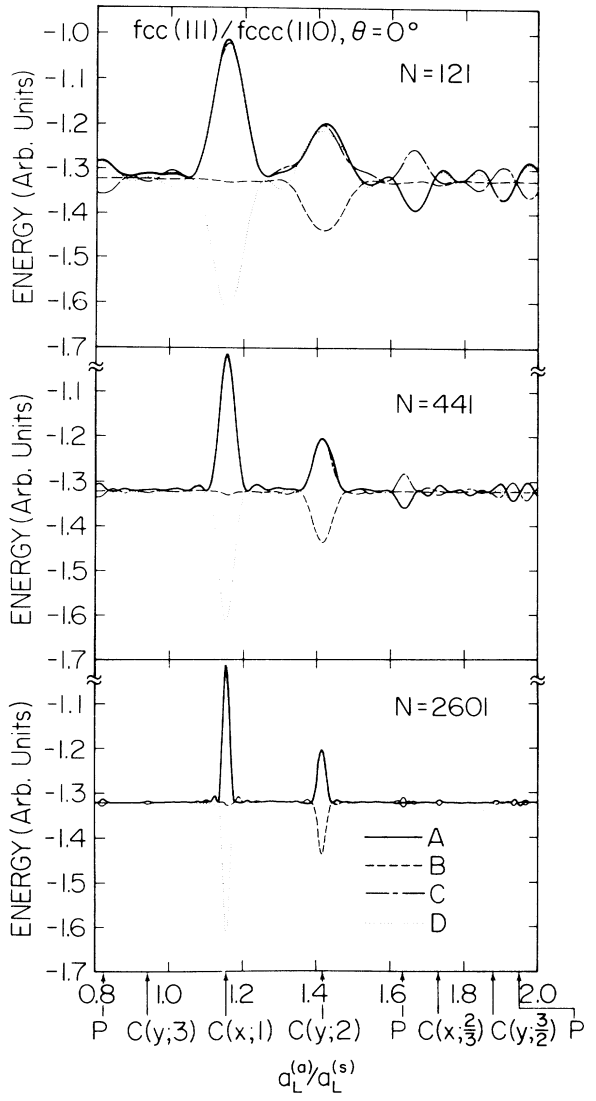

FIG. 7. Energies per adsorbate atom of the system fcc(111)/fcc(110), as a function of lattice-constant ratio $a_L^{(a)}/a_L^{(s)}$, with fixed relative orientation $\theta=0°$, for the total number of adsorbate atoms, $N=121$, 441, and 2601. The energies corresponding to four relative displacements, A, B, C, and D (see Fig. 1) are indicated by solid, dashed, dashed-dotted, and dotted lines, respectively. $C(x;1)$ at $a_L^{(a)}/a_L^{(s)}=2/\sqrt{3}\cong 1.15$, $C(x;\frac{2}{3})$ at $\sqrt{3}\cong 1.73$, $C(y;3)$ at $(2\sqrt{2})/3\cong 0.94$, $C(y;2)$ at $\sqrt{2}\cong 1.41$, and $C(y;\frac{3}{2})$ at $(4\sqrt{2})/3\cong 1.89$ indicate the direction and the order of axial commensuration. P at $4/(2\sqrt{3}+\sqrt{2})\cong 0.82$ indicates partial commensuration, in which the projection of ab onto the ξ axis becomes equal to that of $b'd'/2$. P at $8/(2\sqrt{3}+\sqrt{2})\cong 1.64$ indicates partial commensuration, in which the projection of ab onto the ξ axis becomes equal to that of $b'd'$. P at $4/(2\sqrt{3}-\sqrt{2})\cong 1.95$ indicates partial commensuration, in which the projection of bc onto the ξ axis becomes equal to that of $b'd'/2$.

The higher-order commensuration along the η direction occurs when the spacing between ab and cd ($\equiv d^{(a)}$) and the spacing between $a'b'$ and $c'd'$ ($\equiv d^{(s)}$) retain the relationship $2d^{(a)}=3d^{(s)}$, i.e., $a_L^{(a)}/a_L^{(s)}=2$, as indicated by $C(\eta;\frac{2}{3})$ in Fig. 3. Partial commensuration, indicated by P, occurs when $ab=a'b'$, i.e., $a_L^{(a)}/a_L^{(s)}=\sqrt{3}/\sqrt{2}\cong 1.22$, but with incommensuration along both ξ and η directions. The energy values pertaining to $C(\eta;\frac{2}{3})$ and P are very close to the incommensuration energy.

Figure 4 shows the case of $\theta=30°$. We see that axial commensuration can occur in either the x or y direction,

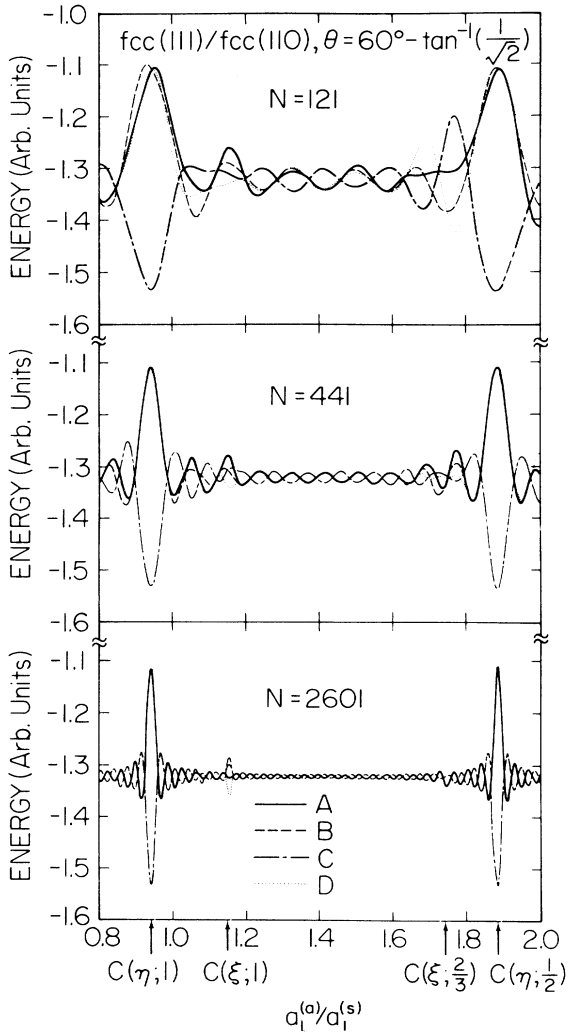

FIG. 8. Energies per adsorbate atom of the system fcc(111)/fcc(110), as a function of lattice-constant ratio $a_L^{(a)}/a_L^{(s)}$, with fixed relative orientation $\theta=60°-\tan^{-1}(1/\sqrt{2})$, for the total number of adsorbate atoms, $N=121$, 441, and 2601. The energies corresponding to four relative displacements, A, B, C, and D (see Fig. 1), are indicated by solid, dashed, dashed-dotted, and dotted lines, respectively. $C(\eta;1)$ at $a_L^{(a)}/a_L^{(s)}=(2\sqrt{2})/3\cong 0.94$, $C(\eta;1/2)$ at $(4\sqrt{2})/3\cong 1.89$, $C(\xi;1)$ at $2/\sqrt{3}\cong 1.15$, and $C(\xi;\frac{2}{3})$ at $\sqrt{3}\cong 1.73$ indicate the direction and the order of axial commensuration.

since ad becomes parallel to $b'd'$, and the adsorbate row perpendicular to ad becomes parallel to $a'c'$. $C(x;2)$ at $a_L^{(a)}/a_L^{(s)}=1$ and $C(x;1)$ at $a_L^{(a)}/a_L^{(s)}=2$ denote that x-axial commensuration for two different orders. The y-axial commensurations occur when $a_L^{(a)}/a_L^{(s)}=2/\sqrt{6}\cong 0.82$, $3/\sqrt{6}\cong 1.22$, and $4/\sqrt{6}\cong 1.63$ as indicated by $C(y;1)$, $C(y;\frac{2}{3})$, and $C(y;\frac{1}{2})$, respectively, in Fig. 4. Partial commensuration can be attained at $a_L^{(a)}/a_L^{(s)}=4/(1+\sqrt{6})\cong 1.16$: the projection of ab (after the 30° rotation) onto the ξ axis becomes equal to that of $a'b'$, but atomic positions are incommensurate in both the x and y directions.

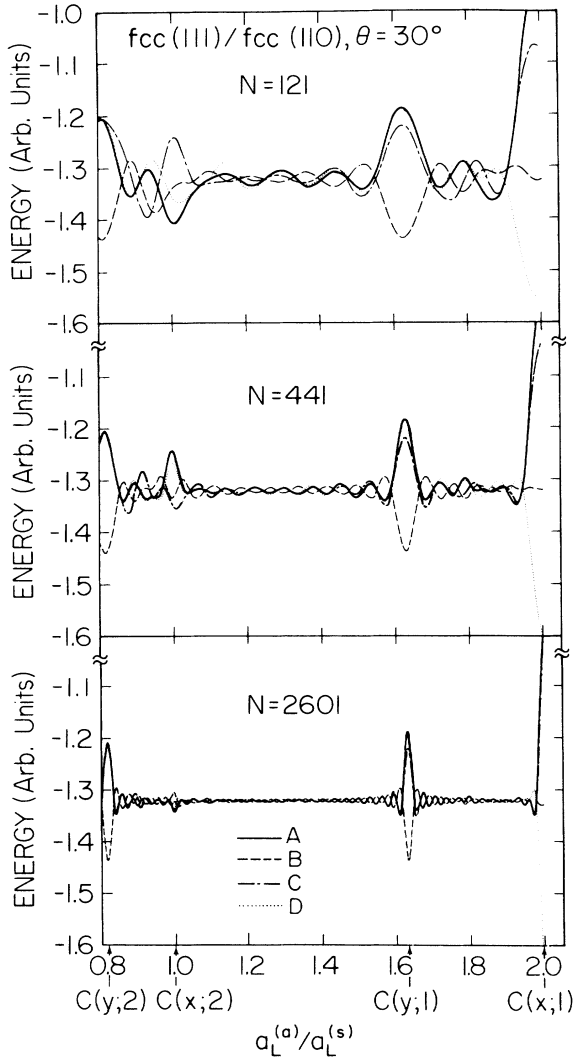

FIG. 9. Energies per adsorbate atom of the system fcc(111)/fcc(110), as a function of lattice-constant ratio $a_L^{(a)}/a_L^{(s)}$, with fixed relative orientation $\theta=30°$, for the total number of adsorbate atoms, $N=121$, 441, and 2601. The energies corresponding to four relative displacements, A, B, C, and D (see Fig. 1), are indicated by solid, dashed, dashed-dotted, and dotted lines, respectively. $C(x;2)$ at $a_L^{(a)}/a_L^{(s)}=1$, $C(x;1)$ at 2, $C(y;2)$ at $2/\sqrt{6}\cong 0.82$, and $C(y;1)$ at $4/\sqrt{6}\cong 1.63$ indicate the direction and the order of axial commensuration.

2. fcc(111)/fcc(001) and fcc(111)/fcc(110)

Based on the analysis of the fcc(111)/bcc(110) system, it is straightforward to investigate the axial commensuration (i.e., eventual coherency) for other types of interfaces composed of two dissimilar structures. First, values for relative orientation θ, which can give rise to axial commensuration, are determined by looking for the geometry in which one set of rows of adsorbate atoms along one particular direction become parallel to that of substrate atoms. For the system fcc(111)/fcc(001), these are $\theta=0°$ and 15°. [$\theta=30°$ is equivalent to $\theta=0°$ due to the C_4 symmetry of fcc(001).] We display the resultant energies corresponding to the above two θ values in Figs. 5 and 6. For fcc(111)/fcc(110), these relative orientations are $\theta=0°$, $60°-\tan^{-1}(1/\sqrt{2})\cong 24.7°$, and 30°: Figs. 7–9 show the corresponding results. It was found that the energy converges at $z\cong 0.63a_L^{(s)}$ above the substrate surface for all cases. As has been used in Figs. 2–4, the notation $C(x;n/m)$, for instance, denotes the crystallographic relationship between the adsorbate and substrate that gives rise to the following axial commensurations: (i) the rows of adsorbate atoms along the y direction are parallel to the rows of substrate atoms; (ii) atomic positions on these rows are incommensurate with each other along the row direction; (iii) these rows form an array in a commensurate fashion along the x direction; and (iv) the spacing between the rows of the adsorbate atoms ($\equiv d^{(a)}$) and the spacing between the rows of the substrate atoms ($\equiv d^{(s)}$) retain the relationship $nd^{(a)}=md^{(s)}$. Occurrence of partial commensuration is indicated by P in the figures, and the relationship between the adsorbate and substrate structure for this case is explained in each of the figure captions.

III. STRAIN AT LATTICE-MISMATCHED INTERFACES

A. Method

In considering strain effects due to lattice mismatch at interfaces, it is essential to include two types of interactions: the adsorbate-substrate and the adsorbate-adsorbate interaction. The former forces all adatoms to be in registry with the substrate (pseudomorphism), whereas the latter tends to keep the adatoms in the equilibrium configuration of the unsupported adsorbate structure. In order to obtain the resulting strain and strain energy, and identify their subsequent roles in the first stage of microcrystallite formation, we consider a rather simplified situation wherein only a homogeneous strain develops in the adsorbate monolayer, and the rigid structure of the substrate is undisturbed. We deal with an interface composed of materials that have the same crystallographic structure but have different natural (unstrained) lattice constants: the relative orientation between the two is thus fixed at zero, and the central atomic position of the adsorbate cluster (relative displacement) is fixed at the position in registry with the substrate. The result of the competition between the adsorbate-adsorbate and adsorbate-substrate interaction is that the lattice constant of the adsorbate attains an intermediate value $b_L^{(a)}$ with an accompanying strain

$e=(b_L^{(a)}-a_L^{(a)})/a_L^{(a)}$, where $a_L^{(a)}$ is the natural (unstrained) lattice constant of the adsorbate material. We define a natural misfit by $P_m=(a_L^{(a)}-a_L^{(s)})/a_L^{(s)}$, where $a_L^{(s)}$ is the natural (unstrained) lattice constant of the substrate. If $b_L^{(a)}=a_L^{(s)}$, the overgrowth is pseudomorphic.

To obtain the total energy of a lattice-mismatched interface, we construct potential functions for both adsorbate-substrate and adsorbate-adsorbate interactions. For the former, we extend the method described in Sec. II to a substrate composed of two types of constituent atoms (anion and cation). By superposing the interatomic potentials in Eq. (4) arising from both anions and cations, the adsorbate-substrate potential function is expressed as

$$V(\mathbf{r})=\sum_{j1} u(|\mathbf{r}-\mathbf{r}_{j1}|;\epsilon_1,\sigma_1)+\sum_{j2} u(|\mathbf{r}-\mathbf{r}_{j2}|;\epsilon_2,\sigma_2)\ , \quad (6)$$

where $\mathbf{r}_{j1}$ and $\mathbf{r}_{j2}$ refer to positions of the substrate atoms in the topmost layer of the anion (cation) sublattice and those in the topmost layer of the cation (anion) sublattice, respectively. As a specific application, we consider the (110) and (001) surfaces of a zinc-blende (ZB) structure. Although a simple two-body interatomic potential as employed here does not naturally give rise to the tetrahedral covalent bonding of a semiconductor from the melt, by artificially specifying atomic positions and crystal symmetry in Eq. (6) and by adjusting parameters accordingly, we attempt to obtain some qualitative information regarding energetics of such systems. As has been done in Sec. II, the quantities $1.12\sigma_1$ and $1.12\sigma_2$ are interpreted as the approximate first- and second-nearest-neighbor bond lengths of the bulk, in the case where adatoms are a constituent of the substrate material (e.g., Ga or As atoms on a GaAs substrate), and surface reconstruction is neglected. It was found, for both ZB(001) and ZB(110), that it takes up to the third Fourier term to confirm energy convergence and the relationships $1.12\sigma_1/a_L^{(s)}\cong\sqrt{3}/4$ and $1.12\sigma_2/a_L^{(s)}\cong\sqrt{2}/2$. The ratio ϵ_2/ϵ_1 was varied between 0.1 and 0.5, and was found to be insignificant in determining the overall functional form of $V(\mathbf{r})$. It is therefore fixed at a value 0.375 throughout. The resulting contour maps are displayed in Figs. 10 and 11 for ZB(110) and ZB(001), respectively. These are the substrate potentials (in arbitrary units) experienced by a single adatom at bulk interplanar distance, $z=(\sqrt{2}/2)a_L^{(s)}$ for ZB(110) and $z=0.25a_L^{(s)}$ for ZB(001). It is seen that the potential minima are located at appropriate positions so that mutually noninteracting adatoms can sit at positions that are in registry with the unreconstructed substrate surface. The potential strength is found to be sensitive to the distance from the surface. For example, at $z=0.35a_L^{(s)}$ above the ZB(001) surface, the maximum value is $\cong 3.0$, and the minimum value is $\cong -2.2$ in the same units as in Fig. 11.

The adsorbate-adsorbate potential function can be obtained in a similar fashion as above, except that the role of substrate atoms is formally replaced by that of "virtual-adsorbate atoms." The configuration of the virtual-adsorbate atoms, in the present model, has the same symmetry as that of the adsorbate atoms, which are now fixed in registry with the virtual adsorbate on compression, expansion, and translation. This model may be visualized as a two-dimensional array of mutually noninteracting balls embedded in an elastic sheet. When the array is compressed or expanded weakly by some external force, the adsorbate atoms will oscillate harmonically near the positions of the virtual-adsorbate potential minima. On the other hand, if the array is strongly compressed, the adsorbate atoms experience the strong repulsive core of

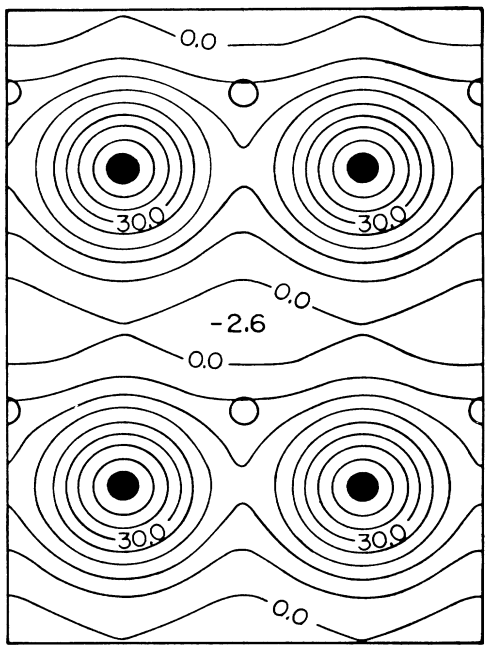

FIG. 10. Contour map of the substrate potential for an unreconstructed ZB(110) surface (with arbitrary units). Open and solid circles refer to positions of the first- and second-nearest-neighbor substrate atoms with respect to an adatom in registry.

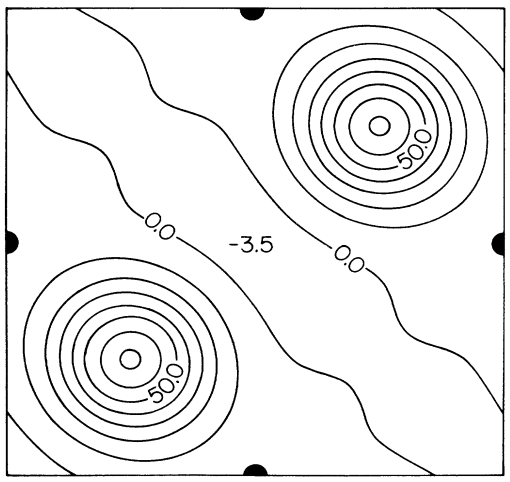

FIG. 11. Contour map of the substrate potential for an unreconstructed ZB(001) surface (with arbitrary units). Open and solid circles refer to positions of the first- and second-nearest-neighbor substrate atoms with respect to an adatom in registry.

the nearby virtual-adsorbate atoms; and if it is strongly expanded, the adsorbate atoms experience the shallow (almost zero) attractive potential arising from the long-range tail of the virtual-adsorbate potential, resulting in almost-free adatoms. The adsorbate-adsorbate potential function in this model is thus expressed in a form similar to Eq. (6), but keeping only the first term, where $\mathbf{r}_j$ now refers to the position of a virtual adsorbate atom. The quantity 1.12σ is now interpreted as the approximate distance between the adsorbate atom and the virtual adsorbate atom in a unit cell. For the case of an fcc(110) adsorbate monolayer in equilibrium, it was found that it takes up to the fourth Fourier term to attain the relationship: $1.12\sigma/a_L^{(a)} \cong \sqrt{6}/4$. For the case of an fcc(001) monolayer, it takes up to the third Fourier term to confirm the relationship: $1.12\sigma/a_L^{(a)} \cong 0.5$. As seen above, effects that arise from beyond the harmonic approximation are easily included in the present model. Inclusion of only the harmonic term in the adsorbate-adsorbate interaction can be found, for example, in Refs. 1, 24, and 30.

For the adsorbate-substrate potential energy we treat the difference in energy between having an adatom at the potential minimum and having it at the maximum as an adjustable parameter (denoted by ϵ_{as}). On the other hand, for the adsorbate-adsorbate potential energy, we treat the energy gain of the equilibrium (unstrained) adsorbate monolayer with respect to free adatoms as an adjustable parameter (denoted by ϵ_{aa}). Note that ϵ_{aa} thus represents the dissociation energy of the unsupported adsorbate monolayer. We vary both ϵ_{as} and ϵ_{aa} between 1 and 5 eV, roughly in concurrence with the order of magnitude of predicted bond energy and cohesive energy for III-V materials.[31,32] A quantitative listing of energy values, however, is beyond the scope of the present calculation: energy units used hereafter are therefore chosen for the sake of convenience in making comparisons.

In spite of the controversial issue[10–15,32] as to what the adsorbate sites are and what the most stable configuration of an adsorbate film on a semiconductor substrate is, the adsorbate monolayer is assumed to be in an fcc(110) structure [onto ZB(110)] or an fcc(001) structure [onto ZB(001)]. Furthermore, we assume that the substrate surface is unreconstructed and rigid. These assumptions in the present calculation are therefore tantamount to emphasizing the strong interaction between the adatoms and the substrate atoms, and assuming that the transition from the substrate material (e.g., GaAs) to the adsorbate material (e.g., AlAs) occurs within a monolayer, preserving the zinc-blende structure throughout.

B. Results and discussion

In the earlier work of Frank and van der Merwe,[1] the critical misfit above which epitaxy should not occur was estimated as $P_m \cong 14\%$, assuming equal interatomic forces in the adsorbate and across the interface. A similar analysis, but using the potential functions obtained in Sec. III A, can be carried out in the present calculation. However, due to the current lack of precise knowledge on the nature and strength of interatomic potentials as well as due to the apparent size dependence of energies (see Sec. II B), it would be difficult to obtain a reasonable estimate of such a critical misfit in general. In this paper, instead, we use the measure of interatomic forces ϵ_{aa} and ϵ_{as}, as parameters, and consider the effects of strain on epitaxy for the cases of small misfit and large misfit (both positive and negative).

The strain that could develop at interfaces composed of lattice-mismatched materials can be read off from the strain value pertaining to the minimum of the resulting total energy (adsorbate-adsorbate potential energy E_{aa} plus adsorbate-substrate potential energy E_{as}). In Fig. 12, we show our results for an fcc(110)/ZB(110) interface composed of materials with a small lattice mismatch $a_L^{(s)}/a_L^{(a)} = 1.005$. Both E_{aa} (dashed line) and E_{as} (dashed-dotted line) are measured with respect to their own minima. The total energy (solid line) is the summation of the two. This is the case of $\epsilon_{aa} = \epsilon_{as} = 2$ eV for three different cluster sizes (total number of adsorbate

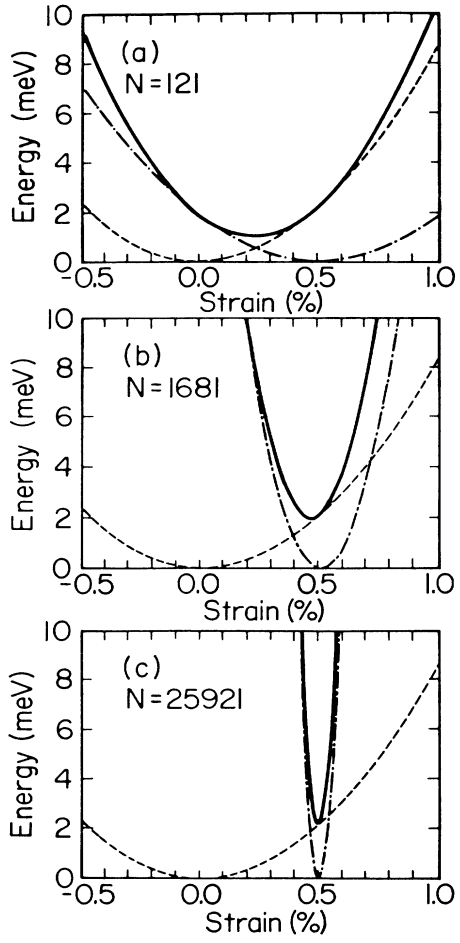

FIG. 12. Adsorbate-adsorbate potential energy (dashed line), adsorbate-substrate potential energy (dashed-dotted line), and total energy (solid line) per adsorbate atom, as a function of strain for a lattice-mismatched interface having natural (unstrained) lattice-constant ratio, $a_L^{(s)}/a_L^{(a)} = 1.005$. The total number of adsorbate atoms is 121 in (a), 1681 in (b), and 25 921 in (c).

atoms, N, being 121, 1681, and 25 921). It is seen in the figure that while the adsorbate-substrate interaction acts to reduce the misfit so as to force all the adatoms to sit in registry with the substrate, the adsorbate-adsorbate interaction counteracts this tendency. Therefore, the minimum value of the total energy with respect to the zero of E_{aa} is the strain energy attained in the adsorbate monolayer. We note that E_{aa} obviously does not depend on N, since the number density is kept the same. In contrast, E_{as} depends sensitively on size as has been analyzed in detail in Sec. II. The size dependence of the latter, therefore, gives rise to size-dependent strain and strain energy. To illustrate this point, we plot values of the strain pertaining to the minimum of total energy as a function of $\sqrt{N}$ for three different sets of ϵ_{aa} and ϵ_{as}. In Fig. 13, we note that the stronger the adsorbate-substrate interaction, the smaller the cluster necessary for perfect pseudomorphism to be attained. (In the present case with $a_L^{(s)}/a_L^{(a)}=1.005$, perfect pseudomorphism implies that the adsorbate film is expanded by 0.5% to come into registry with the substrate.) The above result may be explained as follows. As an adsorbate cluster grows in size, it experiences increasingly strong adsorbate-substrate forces that tend to pull it into registry. [This can be seen from the variation in full width at half maximum (FWHM) of E_{as} in Fig. 12.] This tendency will be amplified further in the case of strong adsorbate-substrate interaction (i.e., larger ϵ_{as}). Pseudomorphism for this case will therefore be realized at early stage of cluster growth. By further varying ϵ_{aa} and ϵ_{as}, we found that the critical adsorbate size N_c, for the onset of pseudomorphism, is linearly dependent on the ratio $\epsilon_{aa}/\epsilon_{as}$:

$$N_c \cong 15\,000\epsilon_{aa}/\epsilon_{as} \tag{7}$$

for fcc(110)/ZB(110). For fcc(001)/ZB(001), the proportional constant was found to be $\cong 21\,000$.

The importance of the critical size, N_c, in interface formation is twofold. Firstly, as can be seen from the saturation behavior of the strain value with increasing N, when an adsorbate cluster reaches N_c it becomes stable to the addition of other adatoms. (In contrast, both strain and strain energy vary appreciably with size for clusters smaller than N_c.) Secondly, N_c sets up a situation for either dislocation formation ($N<N_c$) or perfect coherency ($N>N_c$) in the eventual coalescence. This is because, if $N<N_c$, the edge of each cluster is dislocated from the registry position so that the boundaries between two such clusters will not match up smoothly. The original misfit, for this case ($N<N_c$), is accommodated partially by dislocations and partially by the strain, resulting in an incoherent, low-quality film. On the other hand, if $N>N_c$,

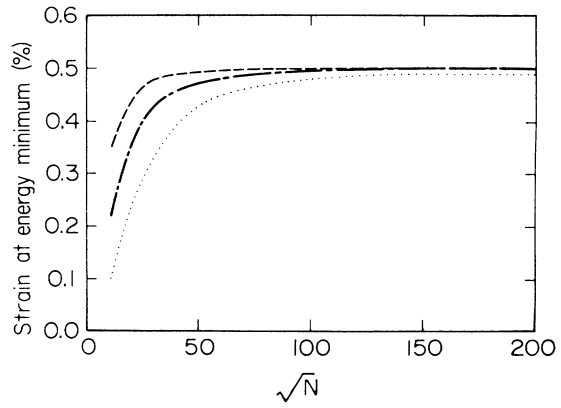

FIG. 13. Strain at total energy minimum as a function of square root of the total number of adsorbate atoms, for $(\epsilon_{aa},\epsilon_{as})=(1,3)$, (2,2), and (3,1) eV, as indicated by dashed, dashed-dotted, and dotted lines, respectively.

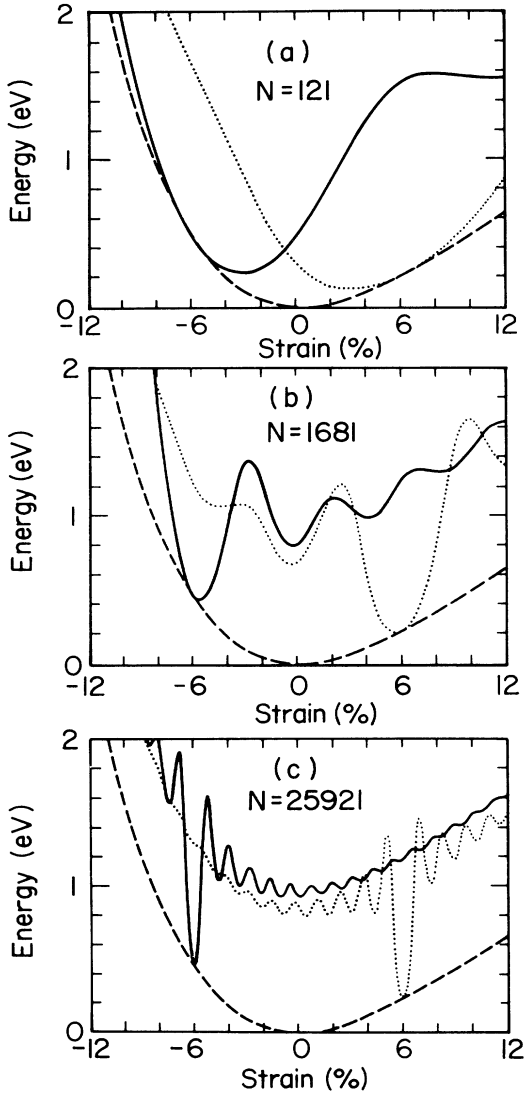

FIG. 14. Total energy for an interface with positive misfit $(a_L^{(s)}/a_L^{(a)}=0.94$, solid line), total energy for an interface with negative misfit $(a_L^{(s)}/a_L^{(a)}=1.06$, dotted line), and adsorbate-adsorbate potential energy (dashed line) as a function of strain, for $(\epsilon_{aa},\epsilon_{as})=(2,3)$ eV. The total number of adsorbate atoms is 121 in (a), 1681 in (b), and 25 921 in (c).

the original misfit is entirely accommodated in the strain without any dislocations. Therefore, our results indicate that, of all the clusters that have formed on the substrate, only those which have reached the critical size N_c will contribute to form the uniform epitaxial film.

It is interesting to note that our numerical results put forward a linear dependence of N_c on $\epsilon_{aa}/\epsilon_{as}$ [Eq. (7)]: the stronger the adsorbate-substrate interaction, the easier it is to obtain a coherent adsorbate film. This is consistent with the fact that the GaAs(001) surface is empirically known to be a more appropriate substrate for epitaxy than the cleaved GaAs(110) surface. One reason could be that the adsorbate-substrate interaction is stronger on the (001) surface than the (110), since the topmost layer of the (001) surface consists of either all cations or all anions, giving rise to strong dangling bonds that can attract adatoms, whereas both anions and cations have coplanar sites on the (110) surface.

In case of small lattice mismatch, the range of strain is limited to be near 0%. As can be seen from Fig. 12, the dependence of E_{aa} on strain is essentially quadratic in this region. Therefore the strain energy in the usual continuum limit, $E_{\text{strain}} \propto e^2$, holds for the small lattice-mismatched interfaces. We emphasize, however, that the strain e itself depends on the size of the cluster (Fig. 13).

We now consider large-mismatched interfaces. Effects arising from anharmonicity in the adsorbate are important here. In Fig. 14 we display the resulting total energies for $a_L^{(s)}/a_L^{(a)}=1.06$ (dotted line) and for $a_L^{(s)}/a_L^{(a)}=0.94$ (solid line) along with the adsorbate-adsorbate energy (dashed line). The case of fcc(110)/ZB(110) is shown with $(\epsilon_{aa},\epsilon_{as})=(2,3)$ eV. We immediately notice the difference in the value of the total energy minimum between the positive misfit $(a_L^{(s)}/a_L^{(a)}=0.94)$ and the negative misfit $(a_L^{(s)}/a_L^{(a)}=1.06)$. This is because when $P_m>0$ the substrate has to compete with the stronger branch of the adsorbate-adsorbate energy in order to press the adsorbate into registry. The resultant strain and strain energy are plotted in Figs. 15 and 16, respectively as a function of $\sqrt{N}$. The size dependence of the strain for the positive and negative misfit is seen to be symmetric in Fig. 15, giving the same critical size N_c for the onset of pseudomorphism. Therefore, as far as first-monolayer formation is concerned, pseudomorphism would occur in an identical fashion for both negative and positive misfit. However, the strain energy exhibits a large difference between the two cases, as is evident from Fig. 16, due to the anharmonic forces in the adsorbate film. The strain energy (per unit interfacial area) in the continuum limit is given by $E_{\text{strain}}=Yte^2$, where Y is a generalized elastic constant, t is the thickness of the overgrowth, and e is the strain. Our results indicate that Y is larger for positive misfit than negative misfit. If the strain energy per monolayer is small, one can expect that a large number of layers will grow pseudomorphically. However, the large value of Y for the positive misfit would give a substantially reduced value of t_c, the critical thickness beyond which pseudomorphism is not possible. Thus one can conclude that, due to the anharmonicity of the adsorbate interatomic forces, a pseudomorphic growth of the deposit would be achieved more readily if the natural lattice constant of the adsorbate is smaller than that of the substrate. Our results also have a direct bearing on the growth of superlattices made up of lattice mismatched materials. For example, in the fabrication of a superlattice composed of Si and Ge_xSi_{1-x}, where $a_L^{(Si)}<a_L^{(Ge_xSi_{1-x})}$, we recommend that the thickness of a Ge_xSi_{1-x} layer be made smaller than that of a Si layer in order to avoid substantial dislocation formation.

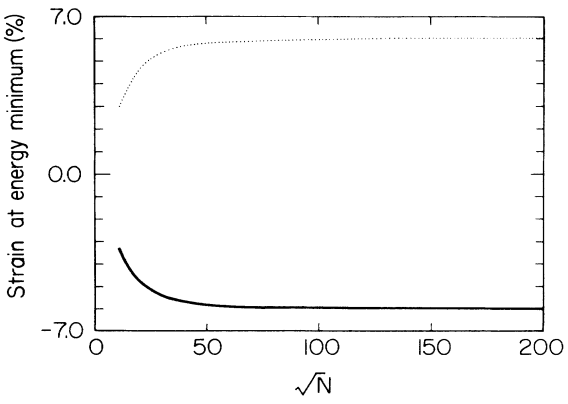

FIG. 15. Strain at total energy minimum as a function of square root of the total number of adsorbate atoms, for $(\epsilon_{aa},\epsilon_{as})=(2,3)$ eV. The solid and dashed lines refer to the cases of positive misfit $(a_L^{(s)}/a_L^{(a)}=0.94)$ and negative misfit $(a_L^{(s)}/a_L^{(a)}=1.06)$, respectively.

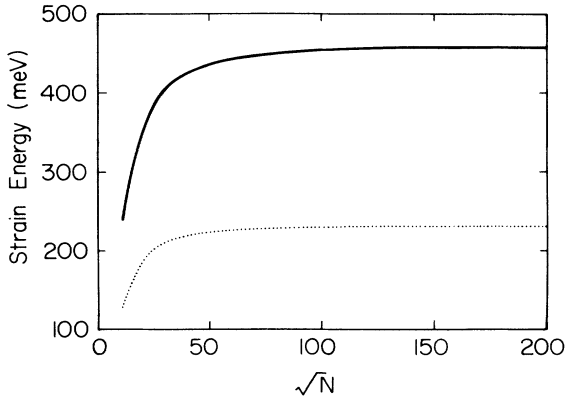

FIG. 16. Strain energy as a function of square root of the total number of adsorbate atoms, for $(\epsilon_{aa},\epsilon_{as})=(2,3)$ eV. The solid and dashed lines refer to the cases of positive misfit $(a_L^{(s)}/a_L^{(a)}=0.94)$ and negative misfit $(a_L^{(s)}/a_L^{(a)}=1.06)$, respectively.

IV. CONCLUSIONS

Static energies for an interface composed of two dissimilar structures (that differ in symmetry) are calculated within the rigid-lattice approximation. The conditions necessary in order to attain a coherent interface are investigated in terms of axial commensuration, by analyzing the dependence of energy on the lattice-constant ratio, rel-

ative orientation and relative displacement between the two structures, as well as the dependence on adsorbate-cluster size.

Strain and strain energy at lattice-mismatched interfaces are studied by including an anharmonic contribution in the adsorbate-adsorbate interaction. The nucleation size of stable microcrystallites is obtained by determining the critical adsorbate-cluster size for the onset of pseudomorphism. The difference in epitaxial growth between positive misfit and negative misfit is explained in terms of anharmonic forces in the adsorbate film with the conclusion that, for better epitaxial growth, the lattice constant of the adsorbate material should be smaller than that of the substrate if lattice mismatched materials are being used. In this regard, it can be recommended that, in the fabrication of superlattice composed of materials A and B (with $a_L^{(A)} < a_L^B$), the thickness of a B layer be made smaller than that of an A layer.

As described earlier, our calculations are based on model potentials (see Secs. II A and III A). The results presented here should therefore be viewed with caution if detailed aspects of semiconductor growth are of concern. However, we would like to mention that most of our results are essentially independent of details of the potentials, and thus should serve as guidelines toward a qualitative understanding of growth problems in general.

Note added in proof. After submission of this manuscript for publication, a series of interesting papers[33] by Milchev and Markov were brought to our attention. The effect of anharmonicity in epitaxial interfaces is also considered in these papers.

ACKNOWLEDGMENTS

Stimulating discussions with Sun-Mok Paik are greatly appreciated. This work is supported by the U. S. Office of Naval Research and by the Department of Defense.

[1]F. C. Frank and J. H. van der Merwe, Proc. R. Soc. London, Ser. A **198**, 205 (1949); **198**, 216 (1949); **200**, 125 (1949).
[2]W. A. Steele, Surf. Sci. **36**, 317 (1973).
[3]J. P. McTague and A. D. Novaco, Phys. Rev. B **19**, 5299 (1979).
[4]C. R. Fuselier, J. C. Raich, and N. S. Gillis, Surf. Sci. **92**, 667 (1980).
[5]P. S. Schabes-Retchkiman and J. A. Venables, Surf. Sci. **105**, 536 (1981).
[6]R. J. Gooding, B. Joos, and B. Bergersen, Phys. Rev. B **27**, 7669 (1983).
[7]L. W. Bruch and J. A. Venables, Surf. Sci. **148**, 167 (1984).
[8]L. W. Bruch, Surf. Sci. **150**, 503 (1985).
[9]M. Hanbücken, M. Futamoto, and J. A. Venables, Surf. Sci. **147**, 433 (1984).
[10]I. P. Batra, J. Vac. Sci. Technol. B **2**, 427 (1984); **3**, 750 (1985).
[11]R. Ludeke, L. C. Chang, and L. Esaki, Appl. Phys. Lett. **23**, 201 (1973).
[12]P. Skeath, I. Lindau, C. Y. Su, and W. E. Spicer, J. Vac. Sci. Technol. **19**, 556 (1981).
[13]R. Ludeke and G. Landgren, J. Vac. Sci. Technol. **19**, 667 (1981).
[14]J. Massies and L. T. Linh. Surf. Sci. **114**, 147 (1982).
[15]G. A. Printz, J. M. Ferrari, and M. Goldenberg, Appl. Phys. Lett. **40**, 155 (1982).
[16]L. A. Bruce and H. Jaeger, Philos. Mag. A **38**, 223 (1978).
[17]I. K. Schuller, Phys. Rev. Lett. **44**, 1597 (1980).
[18]S. M. Durbin, J. E. Cunningham, and C. P. Flynn, J. Phys. F **12**, L75 (1982); S. M. Durbin, Ph. D. thesis, University of Illinois, 1983 (unpublished).
[19]R. Ramirez, A. Rahman, and I. K. Schuller, Phys. Rev. B **30**, 6208 (1984).
[20]M. G. Karkut, D. Ariosa, J.-H. Trisone, and O. Fisher, Phys. Rev. B **32**, 4800 (1985).
[21]L. L. Chang, J. Vac. Sci. Technol. B **1**, 120 (1983).
[22]P. L. Gourley and R. M. Biefeld, J. Vac. Sci. Technol. B **1**, 383 (1983).
[23]I. J. Fritz, L. R. Dawson, and T. E. Zipperian, J. Vac. Sci. Technol. B **1**, 387 (1983).
[24]J. H. van der Merwe, Philos. Mag., Ser. A **45**, 127 (1982); **45**, 145 (1982); **45**, 159 (1982); J. H. van der Merwe and M. W. H. Braun, Appl. Surf. Sci. **22/23**, 545 (1985); E. Bauer and J. H. van der Merwe, Phys. Rev. B **33**, 3657 (1986).
[25]D. Walton, J. Chem. Phys. **37**, 2182 (1962).
[26]R. Ludeke, J. Vac. Sci. Technol. B **2**, 400 (1984).
[27]F. Stillinger and T. A. Weber, Phys. Rev. B **31**, 5262 (1985).
[28]R. Biswas and D. R. Hamman, Phys. Rev. Lett. **55**, 2001 (1985).
[29]A. Kobayashi, S.-M. Paik, K. E. Khor, and S. Das Sarma, Surf. Sci. **174**, 48 (1986).
[30]S. C. Ying, Phys. Rev. B **3**, 4160 (1971).
[31]See, for example, W. A. Harrison, *Electronic Structure and the Properties of Solids*, (Freeman, San Francisco, 1980).
[32]J. Ihm and J. d. Joannopoulos, J. Vac. Sci. Technol. **21**, 340 (1982), and references therein.
[33]A. Milchev and I. Markov, Surf. Sci. **136**, 503 (1984); **136**, 519 (1984); **145**, 313 (1984).